DOI: 10.1002/jcc.21959

A Computational Chemist Approach to Gas Sensors: Modeling the Response of SnO_2 to CO, O_2, and H_2O Gases

Jean-Marie Ducéré,[a,b] Anne Hemeryck,*[a,b] Alain Estève,[a,b] Mehdi Djafari Rouhani,[a,b] Georges Landa,[a,b] Philippe Ménini,[a,b] Cyril Tropis,[a,b] André Maisonnat,[c] Pierre Fau,[c] and Bruno Chaudret[c]

A general bottom-up modeling strategy for gas sensor response to CO, O_2, H_2O, and related mixtures exposure is demonstrated. In a first stage, we present first principles calculations that aimed at giving an unprecedented review of basic chemical mechanisms taking place at the sensor surface. Then, simulations of an operating gas sensor are performed via a mesoscopic model derived from calculated density functional theory data into a set of differential equations. Significant presence of catalytic oxidation reaction is highlighted. © 2011 Wiley Periodicals, Inc. J Comput Chem 33: 247–258, 2012

Keywords: electronic structures/processes/mechanism · sensors · structure property relationships

Introduction

Metal oxide or conductometric gas sensors devices have been developed for the past 40 years[1] and since then, they still rely on a rather empirical definition of their composition when a practical application in gas detection is targeted. The material of choice for this application, and despite the evaluation of various metal oxides and combination of metal oxides, is still tin oxide.[2–6]

This situation in the gas sensors area can be interestingly compared with the case of varistor devices based on zinc oxide, for which, in parallel with a considerable amount of research work and published papers, only a mostly empirical research has finally led manufacturers to build their proprietary varistors composition recipes depending on their applications. No clear evidence of the interaction between the numerous doping elements present in a conventional zinc oxide varistor is defined. However, it has recently been concluded by Barsan et al.[7] that it was still possible to improve the level of knowledge in the field of metal oxide gas sensors thanks to the combination of a simultaneous and large set of experimental techniques. The theoretical modeling of the sensor response in combination with experimental results is moreover presented as a real need to better understand the fine chemical mechanisms occurring at the surface of a tin oxide material. With that aim in mind, we introduce here a bottom-up modeling approach aimed at describing the operating gas sensor device in relation with the basic chemistry mechanisms evolved during detection. In this study, we consider tin oxide gas sensor as a model system. Despite a huge scientific literature and the marketing of many industrial products, a deep fundamental understanding of the sensing characteristics and capabilities remain elusive.

The basic detection principle of these gas sensors consists in the change of the sensing layer conductance with gas adsorption. These observed variations of the resistance are due to the chemical catalytic reactions that occur at the tin dioxide surface (reactions between gas molecules and the oxide surface) resulting in the modulation of conduction barriers between the oxide grains. Many assumptions have been described in literature, and some of them have been modeled by basic and kinetic chemical reactions (balance and kinetics of chemisorbed particles) and/or physic laws (activation energies through surface barrier voltage, diffusion-reaction mechanism, Langmuir-Hinshelwood) but also by kinetic Monte Carlo simulation.[8–12]

First principles-based models have also been proposed[13–15] considering a molecular level descriptions of atomistic and molecular surface reactions on catalyst systems, to describe the oxidation current density for instance.[16,17] Using a first-principles-based microkinetic model developed by Dumesic et al. aiming at predicting rates of reversible elementary steps and surface coverages, many catalysis reactions have been studied:[18–20] methanol conversion on zeolite catalyst, n-hexane and hydrogen on platinum catalysts,[18] CO oxidation via O_2, NO and N_2O, the decomposition of N_2O into N_2 and O_2 over Fe-Y and Fe-mordenite, partial oxidation of methane over Y- zeolites,[19] and methanol decomposition on Pt.[20] Our work deals with the exposure of tin dioxide sensing layer [SnO_2(110)] to CO, O_2, H_2O, and mixture of these gases.

In this work, we developed a bottom-up[21,22] model of the sensor operation starting from surface chemical reactions

[a] *J.-M. Ducéré, A. Hemeryck, A. Estève, M. D. Rouhani, G. Landa, P. Ménini, C. Tropis*
CNRS, LAAS, 7 avenue du colonel Roche, F-31077 Toulouse, France
E-mail: hemeryck@laas.fr
[b] *J.-M. Ducéré, A. Hemeryck, A. Estève, M. D. Rouhani, G. Landa, P. Ménini, C. Tropis*
Université de Toulouse, UPS, INSA, INP, ISAE, LAAS; F-31077 Toulouse, France
[c] *A. Maisonnat, P. Fau, B. Chaudret*
CNRS-LCC, 205 route de Narbonne, F-31077 Toulouse, France
Contract/grant sponsor: LAAS-CNRS.

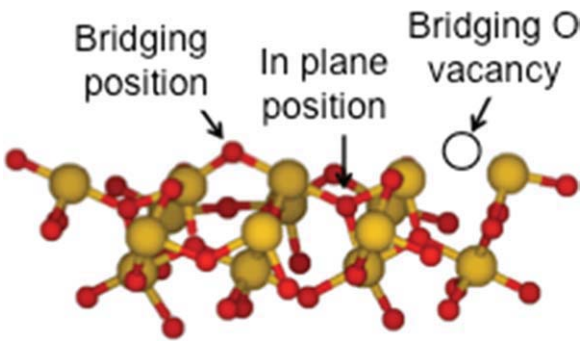

Figure 1. Side view of a SnO_2(101) surface highlighting the bridging and in plane positions of the lattice oxygen atom. A bridging oxygen vacancy is shown. Oxygen atoms are in red and tin atoms are in yellow.

allowing a precise control of further parameterization. Density functional calculations are used to parametrize a mesoscopic model as described in Dumesic's formalism described in Ref. [20]. Both all the characterized atomic-scale chemical reactions occurring at the surface of the sensing layer and the building of the mesoscopic model are described. One specificity of this work lays in a new equation that describes charge transfers occurring in the sensing layer as a function of the adorbates concentrations. The objective is to develop the first tin oxide surface reaction model leading to the transformation of a chemical signal resulting from the surface chemistry to an electrical signal. We also believe that this modeling strategy can provide assistance to the design and development of other types of sensors, both on fabrication technology and detection protocols.

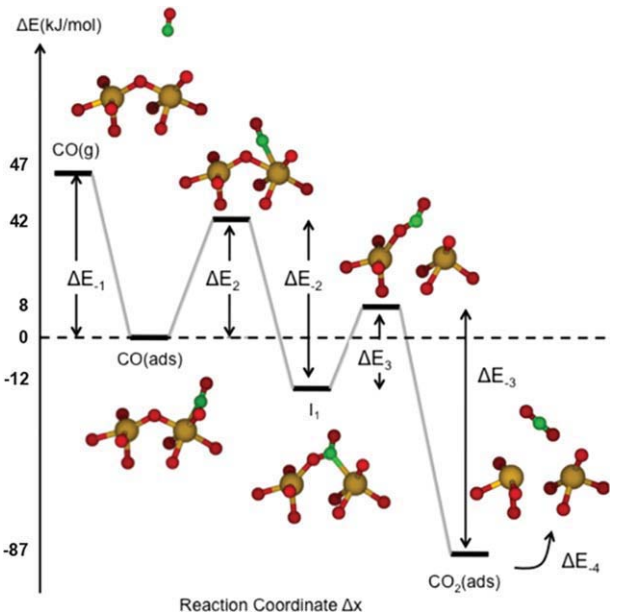

Figure 2. Energetic pathway of the general reaction R.I of CO gas with the SnO_2 surface until the partial reduction of the sensing surface. The energy is plotted against the reaction coordinates. The line is a guide for the eyes. Some side view reduced figures are given at the main steps of the reaction pathway. Oxygen atoms are in red, tin atoms are in yellow, and carbon atoms are in green. The zero reference energy is taken as the CO molecule adsorbed on the surface.

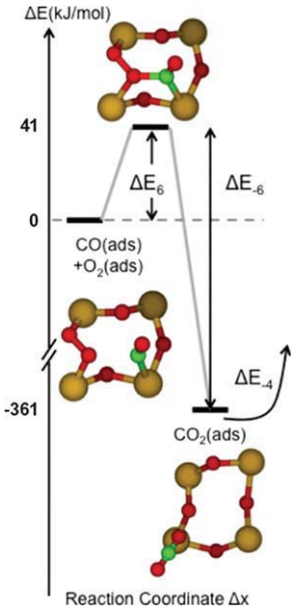

Figure 3. Same as Figure 2, but for reaction R.III describing the reaction between adsorbed CO and adsorbed O_2 species at the surface of the sensing layer. The zero reference energy is taken as both CO and O_2 in an adsorbed form.

Principle of the Multimodel Methodology

First, using static density functional theory (DFT) calculations, we identify and characterize, at the atomic scale, the reactions occurring at the surface of the sensitive layer of the sensor. We characterize the reactions in terms of structures and energies, and we calculate associated charge transfers of each formed surface species.

To simulate the sensors behavior in realistic conditions, the kinetics and, therefore, the temporal evolution of these sensors as a function of external parameters is the main point. A mesoscopic model based on the kinetic rate theory is developed, which requires the knowledge of the reaction parameters. DFT calculations provide all the parameters required by our model, in particular the activation energies and the charge transfers. This methodology, combining DFT calculations and rate equations, leads to a better understanding of the macroscopic gas sensor behavior as a function of the microscopic aspects of the sensing layer.

Physical–Chemical Surface Characterization

Ab initio calculation details

For the understanding of the elementary mechanisms of the various molecules/surface reactions, two clusters are used: a stoichiometric oxide structure ($Sn_{18}O_{59}H_{46}$) cleaved along (101) and a reduced surface $Sn_{18}O_{58}H_{46}$ to mimic a defective surface. Hydrogen atoms are used to passivate the dangling bonds of the cluster. The reduced surface is created by removing a surface oxygen in a bridging position from the stoichiometric SnO_2(101) surface (in opposition to the topmost oxygen atom in plane position, see Fig. 1).[23] The (101) surface is only the second most stable. However, it presents

Table 1. Comparison of the calculated vacancy formation energy and associated charge transfer using the def-TZVP and def2-TZPP basis sets.

	ΔE (kJ mol^{-1})	Charge transfer (e)
def-TZVP	180	−1.098
def2-TZVPP	177	−0.971

the advantage not to undergo complex reconstruction upon hydration or reduction.[24,25] The defined surface layer is large enough to fully reproduce the environment of the central Sn_3O_{13} cluster and so to allow for the reactions between several absorbed species. The surface layer is thus defined as sufficient to achieve adsorption of a molecule and large enough to allow for the reactions between several adsorbed species.

All the calculations are performed using the Turbomole 5.9.[26] suite of programs within the frame of the DFT. We used the gradient-corrected density functional Perdew, Burke and Ernzerhof (PBE),[27] as this functional has been used in a number of previous studies on similar surfaces.[28–36] For the geometry optimizations, we use the def-SVP basis set,[37] which is double-zeta for valence, augmented with a polarization function. Sn atoms [Kr], 4d10 core electrons are treated using Stuttgart pseudopotential.[38] Then, a single point calculation using the Turbomole def-TZVP basis set,[39] which is triple-zeta for valence electrons augmented with a polarization function, is performed on each stationary point to get a more accurate energy and to reduce the basis set superposition error, as Boys and Bernardi's Counterpoise[40] scheme is not well suited to deal with the insertion compounds we are investigating. The resolution of the identity approximation[41] is used to reduce the computational burden. All the stationary points are characterized as minima or transition states through the calculation of the vibrational frequencies. All energy profiles are corrected to account for the zero point energy corrections. The charge transfers are evaluated by the means of the Natural Population Analysis.[42] To validate the adequacy of our basis set, we have calculated the formation energy of a vacancy and its associated charge transfer with the larger def2-TZVPP basis set included in Turbomole,[43] which uses a smaller core ecp for Sn (28 instead of 46 electrons) and includes two polarization shells (up to f for Sn and O) instead of one (up to d for Sn and O). The calculations were performed on the PBE/def-SVP geometries. The comparison is shown is Table 1.

As can be seen, the much more demanding def2-TZVPP does not significantly modify the energy of reaction and only leads to a small decrease of the magnitude of the charge transfer far below the requirements of further multimodel modeling step. Therefore, the def-TZVP basis set appears to be adequate for properly describing both the energetics and the charge transfers.

Identified surface reactions

We consider an ambient atmosphere composed of CO and/or O_2 gases in dry or wet conditions. DFT calculations are used to study the adsorption of gases, the diffusion of adsorbed molecules or atoms, and the subsequent reactions such as the surface reduction on the stoichiometric SnO_2(101) surface. Ten surface reactions have been identified and are listed below. The energies of reaction and activation are gathered in Table 2. These reactions, a combination of adsorption, dissociative chemisorptions are considered as the most important and pertinent ones for what concern their impact on the surface charge redistribution and subsequently a sensor operation. Further mechanisms such as carbonate involving steps, lateral effects, could be included in further DFT investigations; however, their introduction in the set of equation proposed for the macroscopic level of simulation should be only envisaged at the light of their impact versus the tractability of the microkinetic model.

Adsorption of CO(g) on the sensing layer. CO(g) is known to be a reducing gas. Figure 2 presents the complete pathway, starting from the adsorption of the gaseous species [CO(g)] on the surface layer of the sensitive gas sensor, up to the reduction of the SnO_2 surface by CO(g).

At the beginning of the calculation, the two systems, CO(g) and the SnO_2 surface, are considered without interaction, being quite far from each other. The reaction starts by the adsorption of CO(g) on a surface lattice tin atom, noted Sn(l), and results in the creation of an adsorbed CO(ads) species.

$$CO(g) + Sn(l) \leftrightarrow CO(ads) \qquad \text{(R.I.a)}$$

This mechanism requires no activation barrier and is accompanied by an energy gain of 47 kJ mol^{-1} (ΔE_{-1} in Fig. 2); a bond is created between the carbon atom and a surface tin atom. This energy value corresponds to the activation barrier for desorption of CO(ads) from the surface.

The second part of the reaction consists in the diffusion of the adsorbed CO, which reacts with a lattice oxygen atom, noted O(l), of the original sensitive surface, forming an intermediate species (called I_1). This intermediate is characterized by a double bond between C and O.

$$CO(ads) + O(l) \leftrightarrow I_1 \qquad \text{(R.I.b)}$$

The energy gain for this reaction is 12 kJ mol^{-1}, with an activation barrier of 42 kJ mol^{-1} (ΔE_2). The back-reaction to

Table 2. Summary of the reactions, energies of reaction, and activation.

	ΔE	Ea+	Ea−		
$CO(g) + Sn(l) \leftrightarrow CO(ads)$	−47		47	1	R.I.a
$CO(ads) + O(l) \leftrightarrow I_1$	−12	42	54	2	R.I.b
$I_1 \leftrightarrow CO_2(ads) + V$	−75	20	95	3	R.I.c
$CO_2(ads) \leftrightarrow Sn(l) + CO_2(g)$	18	18		4	
$O_2(g) + V \leftrightarrow O_2(ads)$	−98		98	5	R.II
$CO(ads) + O_2(ads) \leftrightarrow CO_2(ads) + O(l)$	−361	41	402	6	R.III
$O_2(ads) + V \leftrightarrow O(l) + O(l)$	−276	36	312	7	R.IV
$CO_2(ads) + O(l) \leftrightarrow CO_2(carb)$	−4	22	26	8	R.V
$H_2O(g) + Sn(l) + O(l) \leftrightarrow OH(ads) + H(ads)$	−150		150	9	R.VI
$OH(ads) + H(ads) + CO(ads) \leftrightarrow I_2$	−42	17	59	10	R.VII.a
$I_2 \leftrightarrow CO_2(ads) + OH(ads) + H(ads) + V$	−60	36	96	11	R.VII.b

All the energies are in kJ mol^{-1}.

Table 3. Structural and energetic values obtained for R.II, R.IV, and R.VI.

	Reaction R.II	Reaction R.IV	Reaction R.VI
Final configuration	O_2 peroxy	SnO_2	OH(ads) + H(ads)
Energy gain (kJ mol^{-1})	106	210	156
Activation barrier (kJ mol^{-1})	0	43	0

These data have been obtained using DFT calculations.

return from I_1 to CO(ads) needs, therefore, an activation barrier of 54 kJ mol^{-1} (ΔE_{-2}).

Then, I_1 transforms into an adsorbed CO_2 molecule on the SnO_2 surface. This mechanism requires an activation energy of only 20 kJ mol^{-1} (ΔE_3), which is low compared with the 59 kJ mol^{-1} gained during the adsorption process and the first diffusion leading to the formation of I_1. Moreover, this last step creates an oxygen vacancy (V) on the surface.

$$I_1 \leftrightarrow CO_2(ads) + V \qquad \text{(R.I.c)}$$

Finally, the adsorbed CO_2 molecule can desorb from the surface with an activation energy of 18 kJ mol^{-1} (ΔE_{-4}). Globally, the reaction of CO(g) with the sensor surface causes a partial reduction of the metal oxide, via a mechanism with high probability of occurrence (low ΔE). This leads to the loss of a SnO_2 lattice oxygen atom[43,44] thus leaving a chemically strong active site. The reduction of the surface leads to fourfold coordinated Sn^{2+}, compared with the sixfold coordinated Sn^{4+} for the stoichiometric surface.

Adsorption of O_2(g) on the sensing layer. The adsorption of O_2(g) on the stoichiometric surface is not favorable,[45] it exhibits that an energy gain of only 6 kJ mol^{-1}. This low energy value favors the rapid desorption of the oxygen molecule, or its rapid migration until it reaches a thermodynamically stable position, for example close to a surface defect. We show, in the following, that this is the case near an oxygen vacancy, in a bridging site of the SnO_2(101) surface.[46] We first consider the case of O_2(g) adsorption on a reduced surface:

$$O_2(g) + V \leftrightarrow O_2(ads) \qquad \text{(R.II)}$$

Here, the oxygen molecule can be directly provided by the gas phase, or can come close to a vacancy after multiple migration steps on the oxide surface. No energetic barrier is required and the energy gain is more than 98 kJ mol^{-1} (ΔE_{-5}) (See Table 3). The adsorbed O_2 molecule in a form of peroxy bridge between the two tin atoms fills the vacancy and stabilizes the system.[45] The oxidation degree of tin atom, initially + II, is increased to an oxidation degree of + IV. Considering the large energy gain obtained during adsorption and the vacancy loss, desorption of the O_2 molecule will be a difficult process.

Reaction between CO(ads) and O_2(ads). Figure 3 displays the reaction pathway between already adsorbed CO and O_2 species, close to each other on the surface.

$$CO(ads) + O_2(ads) \leftrightarrow CO_2(ads) + O(l) \qquad \text{(R.III)}$$

In this reaction which follows R.I and R.II, CO(ads) reacts with one oxygen atom of the peroxy bridge and extracts it from the vacancy. The second oxygen atom of the peroxy bridge, not engaged in the reaction with CO (ads), is free to fully occupy the vacancy and becomes a SnO_2 lattice oxygen atom [O(l)] of the SnO_2 surface. At the end of the reaction, the peroxy bridge containing the O_2(ads) species does not exist anymore, and the vacancy is filled in by an oxygen atom.

This reaction exhibits one pathway toward the reoxygenation of the sensing surface. It requires an activation barrier of 41 kJ mol^{-1} (ΔE_6 in Fig. 3), and stabilizes strongly the starting system with an energy gain of more than 361 kJ mol^{-1}, explained by the surface reoxygenation coupled to the oxidation of carbon monoxide. The back reaction will be a nonfavorable mechanism.

Adsorption of O_2(g) on a divacancy. This reaction follows immediately R.II. The starting system consists in an already adsorbed oxygen molecule on a vacancy, as described in the reaction R.II, close to a second surface vacancy (V).

$$O_2(ads) + V \leftrightarrow O(l) + O(l) \qquad \text{(R.IV)}$$

This reaction is another pathway leading to the reoxygenation of the sensing layer. It is performed, thanks to the second vacancy, close to the peroxy bridge allowing the breaking of this peroxy bridge. In this way, two missing oxygen atoms are regenerated at once. This reaction is probable, with an activation barrier of 36 kJ mol^{-1} (ΔE_7) and an energy gain of more than 276 kJ mol^{-1} by restoring the surface due to the exothermicity of the elementary reaction (Table 3). As presented here, it has a low probability of occurrence at the beginning of the detection process because of the very low concentration of divacancies on the sensing surface. However, as we mentioned above, with the reaction R.I, the surface can be reduced considerably during the CO(g) exposure, leading to an increase of the vacancy concentration on the surface. As the reactions take place, finding two adjacent vacancies becomes possible, favoring the reaction R.IV. Furthermore, this mechanism competes for the reoxygenation of the surface, with R.III which has also a low probability of occurrence at low CO(g) concentrations. Even though its probability is low, this type of reactions is of crucial importance for the overall sensing model as it allows the regeneration of the sensing surface, as a catalytic oxidation.

Reaction of CO_2(ads) species with a SnO_2 lattice oxygen. In this section, we investigate the reaction of an adsorbed CO_2, end product of several reactions (R.I.c, R.II, and R.VII.b) with an oxygen atom of the oxide lattice.

$$CO_2(ads) + O(l) \leftrightarrow CO_2(carb) \qquad \text{(R.V)}$$

This reaction leads to a stable surface species referred to as a surface carbonate configuration. The carbonate configuration[47,48] is composed of three oxygen atoms: two of them coming from the CO_2(ads) and the third atom from the SnO_2 lattice.

Figure 4 shows the complete reaction pathway. The formation of the carbonate species [CO_2(carb)] requires an activation

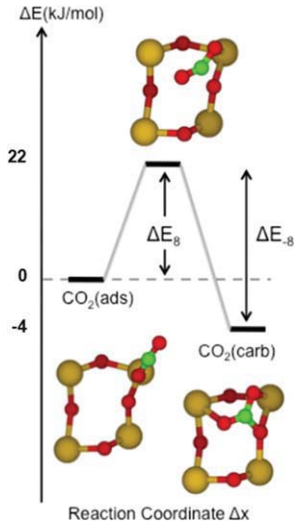

Figure 4. Same as Figures 2 and 3, but for reaction R.V of the transformation of a CO_2 adsorbed species to a surface carbonate conformation. The zero reference energy is taken as the adsorbed CO_2.

energy of 22 kJ mol^{-1} (ΔE_8) and stabilizes weakly the system with an energy gain of 4 kJ mol^{-1}. The back-reaction to destroy CO_2(carb) and to get a CO_2(ads) species is thus a probable mechanism with an activation energy estimated to 26 kJ mol^{-1} (ΔE_{-8}).

Adsorption of H_2O(ads) at the surface of the sensing layer.

$$H_2O(g) + Sn(l) + O(l) \leftrightarrow OH(ads) + H(ads) \qquad (R.VI)$$

Again, the reaction starts with H_2O molecule far from the sensing layer. Taking this reaction into account allows the reproduction of the experiments under wet conditions. Contrary to what was previously observed in the other adsorption processes, the adsorption of a H_2O molecule on the SnO_2 surface requires one tin atom [Sn(l)] and one surface oxygen atom [O(l)]. This adsorption is dissociative,[24,25,49] with H_2O dissociating into two constituents. The first is a hydrogen atom, noted as H(ads), which binds to one surface oxygen atom. The hydrogen atom can only desorb with its lattice oxygen atom, leaving a vacancy behind. The second, noted as OH(ads), binds to a tin surface atom. It can easily desorb from the sensor surface.

This mechanism requires no activation barrier and is very exothermic with more than 150 kJ mol^{-1} (ΔE_9) gained by the system (See Table 3).[24] As shown in Bates'work,[50] a fully dissociated water molecule is more stable than a molecularly adsorbed H_2O species by around 80 kJ mol^{-1}.

Surface reaction between H_2O(ads) and CO(ads). We present here the details of a second reaction involving two species already adsorbed on the surface of the sensing layer, that is, CO(ads) and OH(ads).

$$OH(ads) + H(ads) + CO(ads) \leftrightarrow I_2 \qquad (R.VII.a)$$

This reaction involves a dissociated water molecule OH(ads) + H(ads) as obtained in R.VI, with an adsorbed CO species (the R.I product). It can be decomposed in two steps and leads, at the end of the first step, to an intermediate species noted as I_2. The energetic diagram describing this first step is presented on Figure 5. The reaction starts with the carbon atom of CO(ads) and the oxygen atom of OH(ads) close enough to bind together. For sake of clarity, the reduced slab illustrations only show the OH(ads) fragment of the dissociated water molecule, because it is the only part fully involved in the reaction. But one must keep in mind that a H(ads) species is also present in the neighbourhood. This first step requires an activation energy around 17 kJ mol^{-1} (ΔE_{10}), and is accompanied by a transfer of a proton to a neighbouring lattice oxygen atom O(l) of the SnO_2 lattice, forming an OH bond. The transition state observed in this reaction is similar to what has already been observed in other catalysis studies.[51,52]

Structurally, I_2 is very close to I_1 obtained in R.I. Therefore, as the second step of the reaction, we assume that I_2 can transform into an adsorbed CO_2 species, following the same pathway as in R.I.c.

$$I_2 \leftrightarrow CO_2(ads) + OH(ads) + H(ads) + V \qquad (R.VII.b)$$

The activation energy required for this step is estimated as 36 kJ mol^{-1}. The second step itself is constituted by several elementary mechanisms. However, from the energetic point of view, these mechanisms cannot be dissociated from each other. First, a hydrogen atom is detached from the intermediate I_2 and transforms into H(ads), liberating the CO_2 molecule. Then, the adsorbed hydrogen migrates, together with its neighboring oxygen atom, leaving an oxygen vacancy behind. The migrating OH is finally adsorbed on a surface tin atom [Sn(l)]. The CO_2(ads) can itself desorb from the surface (ΔE_{-4}).

This reaction shows the possible interference between several species, present in the gas phase, on the sensor response. This particular reaction is important in all applications as water is always present in atmospheric environments. Moreover, the role of water is only catalytic as, after reaction with CO, it still remains on the sensor surface. We therefore conclude that

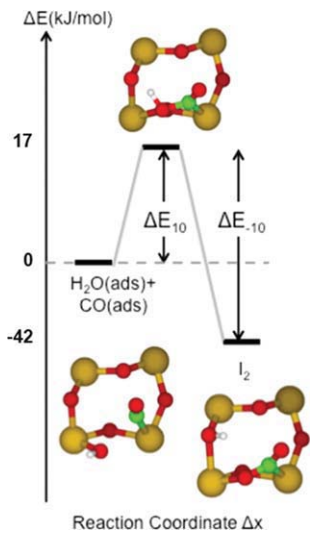

Figure 5. Same as Figures 2 and 3, but for the total reaction R.VII, between adsorbed water and an adsorbed CO leading to the partial reduction of the sensing layer (R.VII.a + R.VII.b). The zero reference energy is taken as both species in adsorbed form.

water should be considered as a pollutant which can compromise the response of the gas sensor toward targeted gases: actually it is shown from literature that water molecules are physisorbed and reduce the active sites on surface.[53,54] Also, gas sensors should be used at high temperatures (>300°C) to avoid water noise effect.[55]

Charge transfers

The detection of adsorbed gases is usually performed via conductivity measurements. The variations of the conductivity are due to charge transfers between the adsorbed species and the sensing layer, resulting in a carrier injection into the oxide that operates as a semiconductor material. For SnO_2, a *n*-type semiconductor in its native form, an electron transfer to the substrate results in an increase of the conductivity. The reverse should be observed for a *p*-type semiconductor. We assume that the charge on the tin atoms determines the conduction of the materials. The zero reference for the charge transfer is considered to be a defectless stoichiometric sensing layer.

DFT calculations allow the quantification of the charge transfers involved in the chemical reactions occurring during the gas detection process, thanks to an analysis of the population of charges. The estimated values of the charge transfers, for all identified surface species, are reported in Table 4. In the case of a reduced surface, where an oxygen atom is removed from the substrate, the surface adopts a Sn valency of +II because the bridging oxygen atom leaves two electrons. The associated charge transfers are strong and have been calculated of more than −1: that is, more than one electron transferred to tin atoms. Experimentally, it is well known that SnO_2 responds to the presence of CO(g) by a large increase of its conductivity due to the partial chemical reduction of the surface of the sensing layer.[5] The calculated charge transfers related to a CO(ads) confirm this trend by showing charge transfers as large as −0.051, by transferring electrons to the sensing layer. In this manner, CO acts as electron donor.[25]

Table 4. Charge transfers ΔCT from each surface species to the surface of the sensing layer.

Surface species	ΔCT [e/site]
SnO_2	0
SnO_2 reduced	−1.098
CO(ads)	−0.051
I_1	−0.342
CO_2(ads)	0.091
CO_2(carb)	0.120
O_2(ads)	−0.063
H_2O(ads)	−0.022
I_2	−0.285

These values have been obtained using *ab initio* calculations.

The physisorption of an oxygen molecule introduces low negative charge transfers (−0.063)[56] due to the weak molecular interactions.[57] The dissociative adsorption of a water molecule provides hydroxyl fragments formation, an increase of the conductivity should be recorded.[24] Indeed, by considering the value of the associated negative charge transfers, hydroxyl species act as electron donors.[58] Finally, we confirm here our previous approximation that I_1 and I_2 are structurally close, showing similar values of charge transfers (see Table 4).

Chemical Rate Theory: Mesoscopic Modeling

In this part, we present a new mesoscopic model that makes it possible to simulate the gas sensor operation in various gas environments under different experimental conditions (temperature, pressure…). For setting up the model, all the DFT structural and energetic data related to local mechanisms are implemented in 11 differential equations based on the chemical kinetic laws.

The characteristic response of the gas sensor is attributable to the evolution of the concentrations of various species present on the surface, and the corresponding charge transfers inducing conductivity variations. These species have been described in Physical–Chemical Surface Characterization section and are noted as: $[CO(ads)]$, $[CO_2(ads)]$, $[I_1]$, $[V]$, $[CO_2(carb)]$, $[O_2(ads)]$, $[Sn(1)]$, $[O(1)]$, $[I_2]$ et $[H_2O(ads)]$, respectively, for the adsorbed CO, the adsorbed CO_2, the intermediate I_1, the vacancies V initially present on the surface or created during the detection process, the carbonated CO_2, the adsorbed O_2, the lattice tin atom, the lattice oxygen atom, the intermediate I_2 and the adsorbed water molecule as OH(ads) + H(ads) form. The model is therefore composed of a set of 10 coupled differential equations, expressing the time evolution of the 10 various species listed above, in interaction with each others.

To establish the set of differential equations, two main types of mechanisms have been considered:"Incoming molecular flux" from the gas phase leading to their adsorption on the surface. This type of mechanism has been used to describe R.I.a, R.II, and R.VI."Reactions" between an adsorbed molecule and the surface species (R.I.b/c, R.IV, R.V) or between two adsorbed species (R.III, R.VII.a/b).

The 'molecular flux" requires no activation energy but depends on the pressure and the temperature of the arriving gas. It will be driven according to the Maxwell Boltzmann statistics as:

$$\Phi_{gas} = C\frac{P_{gas}S}{\sqrt{M_{gas}T_{gas}}} \quad (1)$$

with P_{gas} the partial pressure of the considered gas (in Pa), S the surface of our elementary SnO_2 cell ($S = 1.35 \times 10^{-19}$ m), M_{gas} the molar mass of the gas (in kg mol^{-1}), T_{gas} the gas temperature (K), and C a constant. The above expression is used if a spontaneous adsorption occurs. In cases where an activation energy, from a physisorbed to a chemisorbed state, is observed, the expression is only used to describe the flux towards the physisorbed state. We should remind that, in all cases, the reverse reactions are always taken into account.

In most cases, a reaction requires an activation energy as shown in Physical–Chemical Surface Characterization part. The activation energy of an elementary mechanism can be taken into account by using the Arrhenius' law where the chemical reaction rate is expressed as:

$$k_i = \upsilon \times e^{\frac{-\Delta E_i}{R_g T_{sensor}}} \quad (2)$$

With ΔE_i the activation energy of the mechanism *i* (in J mol^{-1}), R_g the ideal gas constant (8.31 J mol^{-1} K^{-1}) and T_{sensor} the

sensing layer temperature (in K). υ is a dynamic prefactor representing the attempt frequency of jump for the adsorbed species or desorption processes. A unique value estimated at 10^{13} s^{-1} has been attributed to this frequency for all mechanisms.[18] Given the number of detailed *ab initio* calculations carried out in Physical–Chemical Surface Characterization section, including the determination of the zero-point energy (ZPE) and vibrational frequencies, the question of uniqueness of this prefactor may be raised. Indeed, *ab initio* results show that the frequencies depend not only on the mechanisms, but also on the environment, at the atomic scale. Moreover, the actual reaction paths never coincide with the vibrational states. Rather, they are a combination of these states, involving several frequencies at the same time. In this situation, quantum molecular dynamics, discarded here as a result of prohibitive computing times, is the only accurate method of treating the transitions. Using a unique value of the attempt frequency seems therefore a good approximation.

Thus, the elementary mechanisms with lower activation barriers have larger probabilities of occurrence and are the fastest ones.

In addition to the set of 10 coupled differential equations, describing the evolution of the 10 identified species, one more equation reflects the evolution of the charge transfers occurring in the sensing layer during the detection process. This equation sums all charge transfers induced by various species present on the surface. It is written as a weighted sum of the 10 previous equations. Indeed, we are assuming the charge transfer from different species are additive. The weight coefficients in the sum are taken from Table 4. This total charge transfer carriers injected or subtracted from the material by surface reactions and is therefore correlated to the conductivity. It is written as a weighted sum of the 10 previous equations. The weight coefficients in the sum are taken from Table 3.

The final set of 11 equations is expressed as follows:

$$\frac{d[CO(ads)]}{dt} = \underbrace{\Phi_{CO}[Sn(I)]}_{R.I}\ \underbrace{-k_{-1}[CO(ads)] - k_2[CO(ads)][O(I)] + k_{-2}[I_1]}_{R.I}\ \underbrace{-k_6[CO(ads)][O_2(ads)] + k_{-6}[CO_2(ads)][O(I)]}_{R.III}\ \underbrace{-k_{10}[CO(ads)][H_2O(ads)][O(I)] + k_{-10}[I_2]}_{R.VII} \quad (3)$$

$$\frac{d[CO_2(ads)]}{dt} = \underbrace{-k_{-4}[CO_2(ads)]}_{R.I,\ R.III,\ R.V,\ R.VII}\ \underbrace{+k_3[I_1] - k_{-3}[CO_2(ads)][V]}_{R.I}\ \underbrace{+k_{-8}[CO_2(carb)] - k_8[CO_2(ads)][O(I)]}_{R.V}\ \underbrace{+k_6[CO(ads)][O_2(ads)] - k_{-6}[CO_2(ads)][O(I)]}_{R.III}\ \underbrace{-k_{-11}[CO_2(ads)][V][H_2O(ads)] + k_{11}[I_2]}_{R.VII} \quad (4)$$

$$\frac{d[I_1]}{dt} = \underbrace{k_2[CO(ads)][O(I)] - k_{-2}[I_1] - k_3[I_1] + k_{-3}[CO_2(ads)][V]}_{R.I} \quad (5)$$

$$\frac{d[V]}{dt} = \underbrace{-\Phi_{O_2}[V]}_{R.II}\ \underbrace{+k_3[I_1] - k_{-3}[CO_2(ads)][V]}_{R.I} + \underbrace{k_{-5}[O_2(ads)]}_{R.II}\ \underbrace{-k_7[O_2(ads)][V] + k_{-7}[O(I)][O(I)]}_{R.IV}\ \underbrace{-k_{-11}[CO_2(ads)][V][H_2O(ads)] + k_{11}[I_2]}_{R.VII} \quad (6)$$

$$\frac{d[CO_2(carb)]}{dt} = \underbrace{-k_{-8}[CO_2(carb)] + k_8[CO_2(ads)][O(I)]}_{R.V} \quad (7)$$

$$\frac{d[O_2(ads)]}{dt} = \underbrace{\Phi_{O_2}[V] - k_{-5}[O_2(ads)]}_{R.II}\ \underbrace{-k_6[CO(ads)][_2(ads)] + k_{-6}[CO_2(ads)][O(I)]}_{R.III}\ \underbrace{-k_7[O_2(ads)][V] + k_{-7}[O(I)][O(I)]}_{R.IV} \quad (8)$$

$$\frac{d[Sn(I)]}{dt} = \underbrace{-\Phi_{CO}[(I)]}_{R.I} + \underbrace{k_{-1}[CO(ads)]}_{R.I,\ R.III,\ R.VII}\ \underbrace{+k_{-4}[CO_2(ads)]}_{R.I,\ R.III,\ R.V,\ R.VII} + \underbrace{k_{-9}[H_2O(ads)]}_{R.VI,\ R.VII}\ \underbrace{-\Phi_{H_2O}[Sn(I)][O(I)]}_{R.VI} \quad (9)$$

$$\frac{d[O(I)]}{dt} = \underbrace{-k_2[CO(ads)][O(I)] + k_{-2}[I_1]}_{R.I}\ \underbrace{+k_{-8}[CO_2(carb)] - k_8[CO_2(ads)][O(I)]}_{R.V}\ \underbrace{+k_6[CO(ads)][O_2(ads)] - k_{-6}[CO_2(ads)][O(I)]}_{R.III}\ \underbrace{+k_{-9}[H_2O(ads)]}_{R.VI,R.VII}\ \underbrace{-\Phi_{H_2O}[Sn(I)][O(I)]}_{R.VI}\ \underbrace{+2 \times k_7[O_2(ads)][V] - k_{-7}[O(I)][O(I)]}_{R.IV}\ \underbrace{-k_{10}[CO(ads)][H_2O(ads)][O(I)] + k_{-10}[I_2]}_{R.VII} \quad (10)$$

$$\frac{d[H_2O(ads)]}{dt} = \underbrace{\Phi_{H_2O}[Sn(I)][O(I)]}_{R.VI}\ \underbrace{-k_{-9}[H_2O(ads)]}_{R.VI,\ R.VII}\ \underbrace{-k_{10}[CO(ads)][H_2O(ads)][O(I)] + k_{-10}[I_2]}_{R.VII}\ \underbrace{-k_{-11}[CO_2(ads)][V][H_2O(ads)] + k_{11}[I_2]}_{R.VII} \quad (11)$$

$$\frac{d(I_2)}{dt} = \underbrace{k_{10}[CO(ads)][H_2O(ads)][O(I)] - k_{-10}[I_2]}_{R.VII}\ \underbrace{+k_{-11}[CO_2(ads)][V][H_2O(ads)] - k_{11}[I_2]}_{R.VII} \quad (12)$$

$$\frac{d(CT)}{dt} = -0.051 \times \frac{d[CO(ads)]}{dt} + 0.091 \times \frac{d[CO_2(ads)]}{dt} - 0.342 \times \frac{d[I_1]}{dt} - 1.098 \times \frac{d[V]}{dt} + 0.120 \times \frac{d[CO_2(carb)]}{dt} - 0.063 \times \frac{d[O_2(ads)]}{dt} - 0.285 \times \frac{d[I_2]}{dt} - 0.022 \times \frac{d[H_2O(ads)]}{dt} \quad (13)$$

This set of 11 differential equations [from (3) to (13)] constitutes a full model, which is able to describe the behavior of a chemical gas sensor.

Results

Qualitative considerations on the sensor operation

The analysis of the reaction pathways on the surface, calculated via DFT, can lead to a qualitative description of the operation of oxide gas sensors. Indeed, considering reactions R.I, R.II, and R.IV, a complete catalytic cycle may be identified and characterized highlighting the redox properties of the tin dioxide layer on gases exposure.[51,59,60]

This catalytic cycle is summarized by the following main steps:

1. In reaction R.I, a CO(g) species adsorbs on a defectless part of the sensing layer. Then, this CO(ads) species reacts with an oxygen atom of the original SnO_2 lattice to form a CO_2(ads). This process leads to a partial reduction of the surface. Here, the sensing layer looses an oxygen atom.

2. In reaction R.II, the adsorption of an oxygen molecule on the reduced surface fills the vacancy.

3. As the reaction goes along, in dry (see R.I) as well as in wet (see R.VI) conditions, the surface is more and more reduced favoring the creation of vacancies and the occurrence of R.IV. This last reaction will reoxygenate the reduced surface by providing two new oxygen atoms to the SnO_2 lattice.

4. The cycle can continue as in (1), thanks to the yield of oxygen atoms by reactions R.II and R.IV.

The key process in the detection behavior of a semiconductor oxide is the surface ability to respond to the presence of adsorbed oxygen species.[61] In other words, the variable valency of tin of II and IV is the main phenomenon, which explains the gas detection and is responsible for the catalytic activity of the surface. The reduction and the oxidation of the sensing layer take place successively, corresponding to the formation and the annihilation of oxygen vacancies.[62–64]

Indeed, if no oxygen is supplied during the gas detection process, gases such as CO and H_2O will reduce the sensing layer considerably, leading to a full consumption of the lattice oxygen atoms. Finally, the detection process will stop because of the lack of reacting oxygen atoms required by reactions such as R.I, R.VII.a.

The dynamic response of chemical gas sensor

The aim of the simulations is to create all the operating conditions encountered during the use of the sensor in a realistic environment, in terms of temperature, partial pressures of gases, humidity,…). Only DFT data have been implemented in this model, no empirical results has been used. In the simulations presented below, typical conventional experimental conditions are investigated as proposed by Menini and coworkers[65] in response to classical specifications imposed by legislation: (i) CO, detecting 200 ppm requires an evacuation alarm while a 60 ppm low threshold must be also detected, other considered values for O_2/N_2 (20/80%) mixtures and H_2O between 30 and 70% are classical values at ambient temperature; (ii) the temperature of the flowing gas is fixed at 298 K and the sensor surface temperature at 573 K, an average common temperature in applications; and (iii) we also assume that the initial state of the oxide surface contains few vacancies, according to thermodynamic equilibrium law and a calculated formation enthalpy of 187 kJ mol^{-1}.

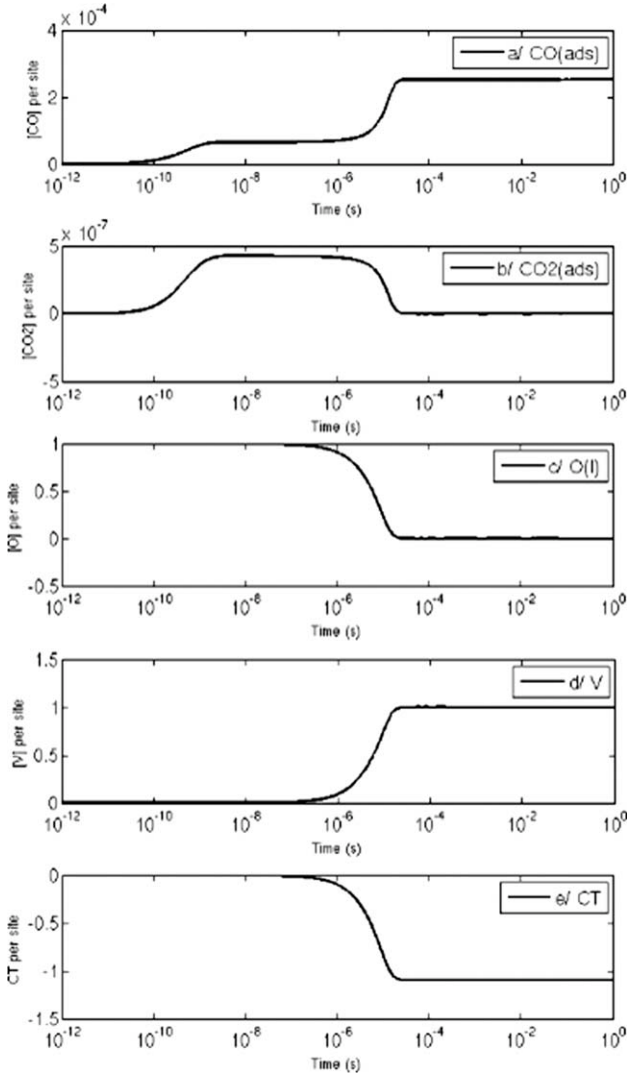

Figure 6. Temporal evolution of the concentrations of various species: CO(ads) (a), CO_2(ads) (b), O(l) (c), and V (d) entities and of charge transfers to the substrate (e). The gas and the substrate temperatures are, respectively, 298 K and 573 K. The atmosphere is composed of only CO(g) at 0.02%.

To distinguish the features of the dynamic response for each gas, and to properly characterize the sensors response, first simulations are performed in the presence of only CO(g). In the following, we will concentrate on few pertinent simulations related to gas mixtures composed of CO, O_2, and H_2O. The Figures 6–8 show the influence of external parameters on the detection efficiency of the SnO_2 sensor.

It is to be pointed that the time scale for the reaction to occur is particularly fast, in the order of each single reaction

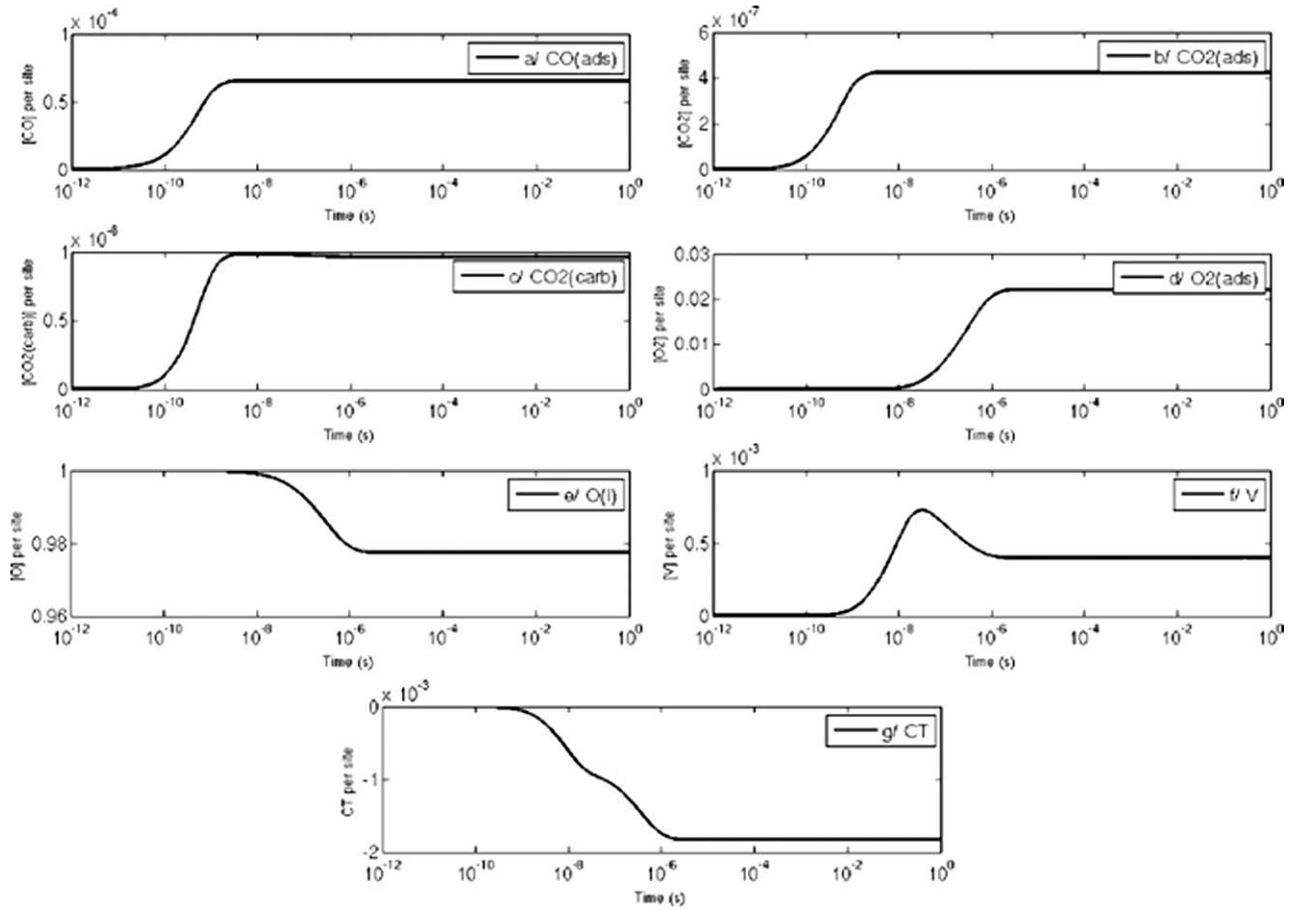

Figure 7. Same as Figure 6, but in an atmosphere containing 20% O_2 in CO(g). Temporal evolution of the following species: CO(ads) (a), CO_2(ads) (b), CO_2(carb) (c), O_2(ads) (d), O(l) (e), and V (f) entities and of charge transfers to the substrate (g).

mechanisms when looking at the temporal evolution curves here after. The additional time scale which accounts for the gas transport is missing here and could be addressed through a feature scale level of modeling. We highlight above the difficulty of this sensor for the detection. Then to model the feature scale of the sensor, one more step in the bottom up strategy must be added shown as the reactor scale modeling.

CO(g) response. In the presence of pure CO gas, the SnO_2 sensor is very reactive as CO can reduce rapidly the sensor surface. The kinetics of the basic mechanisms is shown in Figure 6. The simulations/experiments are performed under nitrogen flux at atmospheric pressure, containing 200 ppm of CO. The partial pressure of CO therefore is of 20 Pa. The nitrogen carrier gas is inactive: its effects have not been considered in the simulations. As can be observed on Figure 6a, CO adsorption takes place in a two stage process. In a first stage, the adsorbed CO molecules are rapidly oxidized, giving rise to CO_2 molecules adsorbed on the substrate surface. This reaction goes through the production of the I_1 intermediate specie, following reactions R.I.a, R.I.b, R.I.c, and R.V. This transformation can be seen on Figure 6b, where an increase of adsorbed CO_2 is observed. We point out that the concentration scales are different in Figures 6a and 6b. This shows that the amount adsorbed CO_2 never exceeds a very small fraction ($\sim 10^{-6}$) of the total coverage. The CO_2 molecules rapidly desorb from the surface. This desorption is concomitant with the depletion of surface oxygen atoms (Fig. 6c) and the creation of oxygen vacancies (Fig. 6d). During this first stage, the concentration level of adsorbed CO_2 remains flat. Once the surface oxygen atoms are deleted, the CO_2 can no more be produced and its concentration drops.

In the second stage, CO molecules still continue to be adsorbed and a second rise of the CO concentration is observed (Fig. 6a). The CO concentration then stabilizes at 10^{-3} per Sn surface site (Fig. 6a), as a result of the equilibrium between the adsorbed gas phases, at the experimental temperature of 573 K and CO partial pressure of 20 Pa.

Thus, in an atmosphere without oxygen, the final surface is fully reduced, with no remaining oxygen atom, and the tin atoms are involved in a bond with a CO(ads) fragment. The observed charge transfers are highly negative (Fig. 6e). For a native *n*-type SnO_2 semiconductor, this results in an increase of the sensor conductivity.

Response to a mixture of CO and O_2. We demonstrated that CO(g) is highly reactive with SnO_2 surface, with a high reducing power. The requirement of an oxygen supply, for a catalytic oxidation, is therefore primordial to regenerate the sensing layer. Knowing the response and the profile for the isolated CO gas, the simulations are now performed for a gas mixture. The simulations/experiments produced here

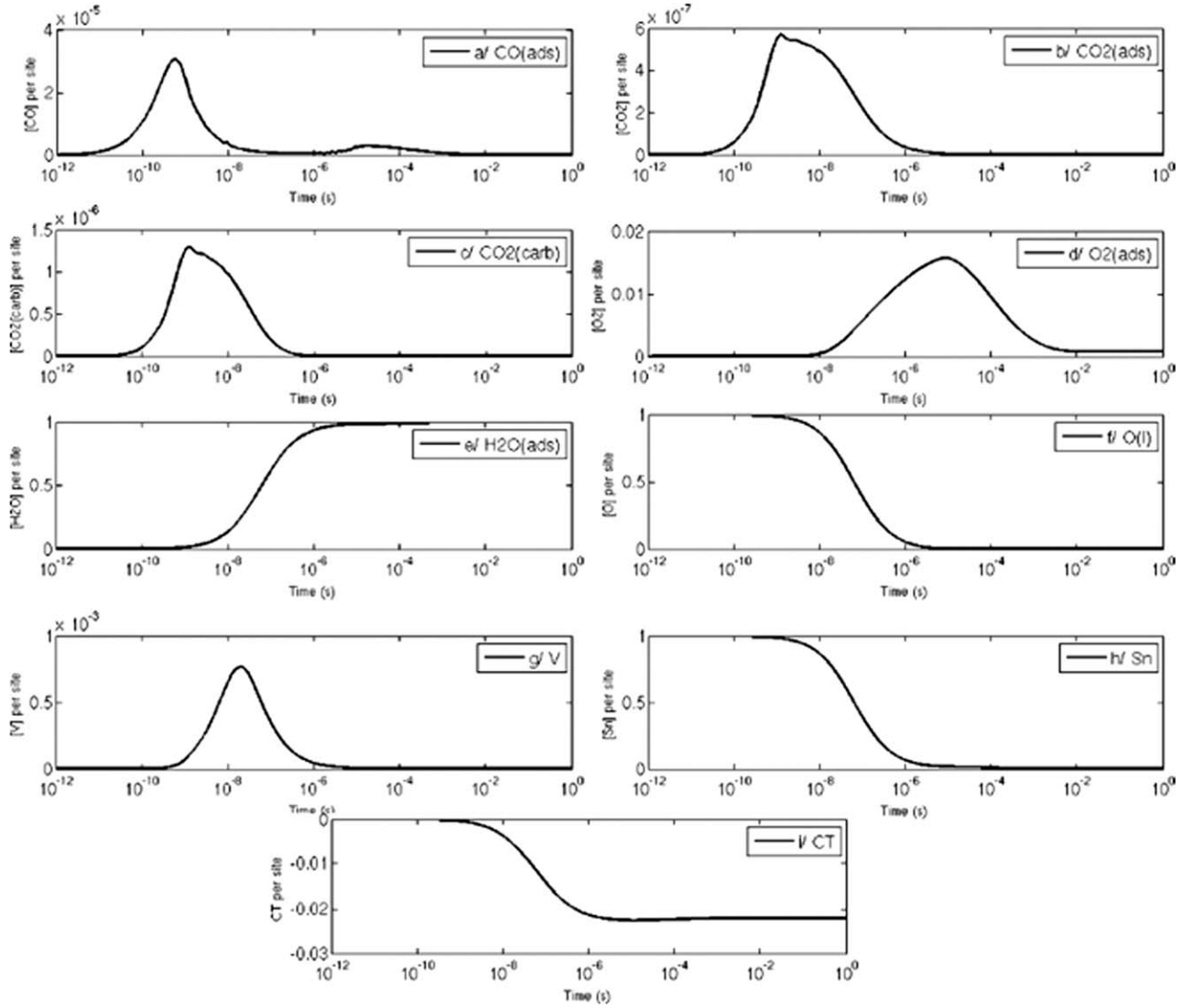

Figure 8. Same as Figure 7, under wet conditions (2% of humidity) for the following species: CO(ads) (a), CO_2(ads) (b), CO_2(carb) (c), O_2(ads) (d), H_2O(ads) (e), O(l) (f), V (g), and Sn(l) (h) entities, and in (i) the charge transfers.

correspond to 200 ppm of CO in an 80% N_2—20% O_2 mixture reproducing the atmospheric composition.

The regeneration process is achieved through the reaction of oxygen molecules adsorbing on surface oxygen vacancies (Reaction R.II). The subsequent reaction of this complex with an adsorbed CO molecule leads to the formation of carbonate specie (Reaction R.V), which is a weakly stable specie. Contrary to the preceding section, the CO detection is performed in a single stage, the concentration of adsorbed CO saturating rapidly to a flat level (Fig. 7a). This concentration level is an order of magnitude lower than in the case of pure CO, as a result of oxygen interaction with the sensor surface. At the same time, the decrease in the concentration of adsorbed CO_2, observed previously, is no more observed. Adsorbed CO_2 concentration stabilizes at a level slightly higher than the previous transient level (Fig. 7b). The carbonate specie is also stabilized at a level an order of magnitude higher than the adsorbed CO_2 concentration (Fig. 7c). The difference between the concentration levels result from the relative stability of the carbonate specie, while the adsorbed CO_2 can rapidly desorb from the surface too.

Another effect of the regeneration mechanism can be observed on Figure 7e which shows the evolution of the lattice oxygen concentration. This concentration decreases very rapidly with respect to its value in perfect SnO_2. Let us remind that oxygen lattice was completely depleted in the absence of oxygen in the gas phase. Here, the oxygen depletion mechanism is compensated by oxygen molecules adsorbing from the gas phase (Fig. 7d). Also, the vacancy concentration increases first, then decreases rapidly, and stabilizes finally at a relatively high level (Fig. 7f). A competition between surface reduction and oxidation is established where the reduction is faster than oxidation.

Finally, complete regeneration of the surface can be achieved if the CO gas flux is interrupted (Fig. 7h). The total charge transfer to the sensor is always negative (Fig. 7g),

leading to an increase of the conductivity of the *n*-type native SnO_2. The conductivity increase is seen to be higher in the presence of oxygen in the ambient atmosphere.

Sensor response in a wet ambient. In addition to oxygen, water is present in all practical applications, often in large proportions. In this section, we simulate the response of the sensor when adding 2% water vapor to the previous mixture, containing already CO, O_2, and N_2. Examination of the sensor response shows two stages. In the first stage, similar effects as those seen in the previous section are observed: adsorption of CO, production of CO_2 by reduction of the sensor surface, regeneration of the surface through atmospheric O_2 adsorption (see Figs. 8a, 8b, and 8d). The concentration levels are also similar to those already observed.

In the second stage, water molecules begin to adsorb on the surface and eventually cover almost completely the sensor surface (Fig. 8e). This strong adsorption is followed by both desorption of CO molecules and CO_2 species (Figs. 8a–8c). In this process, the concentration of adsorbed oxygen molecules drops due to the saturation of relative vacancy active sites on the surface (Fig. 8d).

Finally, the surface is covered by water molecules that are bonded to one lattice oxygen and one Sn atom (Fig. 8h). The remaining second lattice oxygen is still present on the surface (Fig. 8f). Contrary to CO and CO_2 desorption, the oxygen desorption is slow: we observe a slow replacement of adsorbed oxygen by water molecules on the surface that is completely poisoned after this second stage. Experimentally, it is shown that H_2O contributes to the ageing of the gas sensor.[54] This slow trade off can be explained by the important difference between partial pressures of oxygen and water in the incoming flux which contains 20% oxygen and only 2% water.

The sensor conductivity increases strongly (Fig. 8i), compared with the two previous cases, as a result of the large amount of charges injected, by the large number of adsorbed water molecules, into the semiconducting SnO_2 material.

Conclusions

This article presents a first attempt to set up an *ab initio* model for the simulation of a metallic oxide gas sensor response to various gas mixtures and experimental conditions. This model has been developed in the frame of a bottom-up strategy using DFT calculations, for a basic understanding of the interaction of molecular gases with the SnO_2 surface, and using a home-made mesoscopic scale model, which provides information about the dependence of the sensor to the external gas environments.

DFT calculations unravel many stable and metastable surface structures essential to a new understanding of the chemistry taking place at the surface of the gas sensor.

These calculations highlight that

- The behavior of a gas sensor is based on the catalytic oxidation of CO involving successive reduction and reoxidation of the oxide layer.
- The role of the oxygen vacancies for CO detection
- The presence of a carbonate intermediate as a unique CO_2 chemical trace offering a possibility to draw a strategy for further CO_2 detection.

These basic data are used to simulate the sensor operation under various environments. We can observe that all investigated mechanisms, except the oxygen desorption in the presence of water, are very fast compared with the experimental detection sensitivity which is of the order of ms. This means that static detection of specific gases in mixtures would be very difficult. Dynamic detection procedures, involving variable temperature cycles, should therefore be considered in practical applications. Dynamic detection processes may also allow, by increasing the temperature, to clean the sensor surface from all pollutant species, especially water molecules.

The developed model can be further applied to the screening of these experimental dynamical strategies and can be extended to other gas species.

Along the same line, the model can be enhanced by the introduction of new chemical surface reactions among the nonexhaustive list of already identified surface reactions such as the formate formation removing OH species from the surface. At this stage, DFT as well as mesoscale code highlight the difficulty to perform CO_2 detection from pure tin oxide surfaces. We believe that the modeling strategy proposed here can be used to open new routes for gas detection (other oxide surfaces, doping, architectures, and materials).

[1] N. Taguchi, U.S. Pat. 3,631,436, 1971.
[2] G. Korotcenkov, Mater Sci Eng B 2007, 139, 1.
[3] G. Eranna, B. C. Joshi, D. P. Runthala, R. P. Gupta, Crit Rev Solid State 2004, 29, 111.
[4] R. Moos, K. Sahner, M. Fleischer, U. Guth, N. Barsan, U. Weimar, Sensors 2009, 9, 4323.
[5] P. Ménini, F. Parret, M. Guerrero, K. Soulantica, L. Erades, A. Maisonnat, B. Chaudret, Sens Actuators B-Chem 2004, 103, 111.
[6] L. Erades, D. Grandjean, C. Nayral, K. Soulantica, B. Chaudret, P. Menini, F. Parret, A. Maisonnat, New J Chem 2006, 30, 1026.
[7] N. Barsan, D. Koziej, U. Weimar, Sens Actuators B-Chem 2007, 121, 18.
[8] U. Pulkkinen, T. T. Rantala, T. S. Rantatla, V. Lantto, J Mol Catal A-Chem 2001, 166, 15.
[9] T. Rantala, V. Lantto, T. Rantala, Sens Actuators B-Chem 1998, 47, 59.
[10] A. Fort, S. Rocchi, M. B. Serrano-Santos, M. Mugnaini, V. Vignoli, A. Atrei, R. Spinicci, Sens Actuators B-Chem 2006, 116, 43.
[11] V. Brynzari, G. Korotchenkov, S. Dmitriev, Sens Actuators B-Chem 1999, 61, 143.
[12] J. W. Gardner, Semicond Sci Tech 1989, 4, 345.
[13] A. B. Mhadeshwar, J. R. Kitchin, M. A. Barteau, D. G. Vlachos, Catal Lett 2004, 96, 13.
[14] J. K. Nørskov, P. Stoltze, Surf Sci 1987, 189/190, 91.
[15] S. Linic, M. A. Barteau, J Catal 2003, 214, 200.
[16] P. Liu, A. Logadottir, J. K. Nørskov, Electrochim Acta 2003, 48, 3731.
[17] P. Liu, J. K. Nùrskov, Fuel Cells 2001, 1, 192.
[18] J. A. Dumesic, B. A. Milligan, L. A. Greppi, V. R. Balse, K. T. Sarnowski, C. E. Beall, T. Kataoka, D, F. Rudd, A. A. Trevino, Ind Eng Chem Res 1987, 26, 1399.
[19] L. M. Aparicio, J. A. Dumesic, J Mol Catal 1989, 49, 205.
[20] A. A. Gokhale, S. Kandoi, J. P. Greeley, M. Mavrikakis, J. A. Dumesic, Chem Eng Sci 2004, 59, 4679.
[21] A. Hémeryck, A. Estève, N. Richard, M. Djafari Rouhani, G. Landa, Surf Sci 2009, 603, 2132.

[22] G. Mazaleyrat, A. Estève, L. Jeloaica, M. Djafari Rouhani, Comput Mater Sci 2005, 33, 74.
[23] I. Manassidis, J. Goniakowski, L. N. Kantorovich, M. J. Gillan, Surf Sci 1995, 339, 258.
[24] M. Batzill, W. Bergermayer, I. Tanaka, U. Diebold, Surf Sci 2006, 600, L29.
[25] S. H. Hahn, N. Bârsan, U. Weimar, S. G. Ejakov, J. H. Visser, R. E. Soltis, Thin Solid Films 2003, 436, 17.
[26] R. Ahlrichs, M. Bär, M. Häser, H. Horn, C. Kölmel, Chem Phys Lett 1989, 162, 165.
[27] J. P. Perdew, K. Burke, M. Ernzerhof, Phys Rev Lett 1996, 77, 3865.
[28] C. Zhou, J. Li, S. Chen, J. Wu, K. R. Heier, H. Cheng, J Phys Chem C 2008, 112, 14015.
[29] A. V. Bandura, J. D. Kubicki, J. O. Sofo, J Phys Chem B 2008, 112, 11616.
[30] M. Viitala, O. Cramariuc, T. T. Rantala, V. Golovanov, Surf Sci 2008, 602, 3038.
[31] M. Epifani, J. D. Prades, E. Comini, E. Pellicer, M. Avella, P. Siciliano, G. Faglia, A. Cirera, R. Scotti, F. Morazzoni, J. R. Morante, J Phys Chem C 2008, 112, 19540.
[32] M. Epifani, J. D. Prades, E. Comini, A. Cirera, P. Siciliano, G. Fagliac, J. R. Morante, Phys Chem Chem Phys 2009, 11, 3634.
[33] Y. B. Xue, Z. A. Tang, Sens Actuators B 2009, 138, 108.
[34] Z. Zhu, R. C. Deka, A. Chutia, R. Sahnoun, H. Tsuboi, M. Koyama, N. Hatakeyama, A. Endou, H. Takaba, C. A. Del Carpio, M. Kubo, A. Miyamoto, J Phys Chem Solids 2009, 70, 1248.
[35] P. J. Hotchkiss, H. Li, P. B. Paramonov, S. A. Paniagua, S. C. Jones, N. R. Armstrong, J.-L. Brédas, S. R. Marder, Adv Mater 2009, 21, 4496.
[36] Z. Wen, L. Tian-Mo, L. Xiao-Fei, Phys B 2010, 405, 3458.
[37] A. Schäfer, H. Horn, R. Ahlrichs, J Chem Phys 1992, 97, 2571.
[38] G. Igel-Mann, H. Stoll, H. Preuss, Mol Phys 1988, 65, 1321.
[39] A. Schäfer, C. Huber, R. Ahlrichs, J Chem Phys 1994, 100, 5829.
[40] S. F. Boys, F. Bernardi, Mol Phys 1970, 19, 553.
[41] K. Eichkorn, F. Weigend, O. Treutler, R. Ahlrichs, Theor Chem Acc 1997, 97, 119.
[42] A. E. Reed, R. B. Weinstock, F. Weinhold, J Chem Phys 1985, 83, 735.
[43] F. Weigend, R. Ahlrichs, Phys Chem Chem Phys 2005, 7, 3297.
[44] M. Batzill, K. Katsiev, J. M. Burst, U. Diebold, A. M. Chaka, B. Delley, Phys Rev B 2005, 72, 165414.
[45] M. Batzill, U. Diebold, Phys Chem Chem Phys 2007, 9, 2307.
[46] A. Maiti, J. A. Rodriguez, M. Law, P. Kung, J. R. McKinney, P. Yang, Nano Lett 2003, 3, 1025.
[47] J. Oviedo, M. J. Gillan, Surf Sci 2001, 490, 221.
[48] M. Melle-Franco, G. Pacchioni, A. V. Chadwick, Surf Sci 2001, 478, 25.
[49] S. Emiroglu, N. Bârsan, U. Weimar, V. Hoffmann, Thin Solid Films 2001, 391, 176.
[50] J. Goniakowski, M. J. Gillan, Surf Sci 1996, 350, 145.
[51] S. P. Bates, Surf Sci 2002, 512, 29.
[52] C. T. Campbell, K. A. Dauber, J Catal 1987, 104, 19.
[53] N. Schumacher, A. Boisen, S. Dahl, A. A. Gokhale, S. Kandoi, L. C. Grabow, J. A. Dumesic, M. Mavrikakis, I. Chorkendorff, J Catal 2005, 229, 265.
[54] D. S. Vlachos, P. D. Skafidas, J. N. Avaritsiotis, Appl Phys Lett 1993, 63, 1760.
[55] R. Ionescu, Sens Actuators B-Chem 1999, 58, 375.
[56] G. Korotchenkov, V. Brynzari, S. Dmitriev, Sens Actuators B-Chem 1999, 54, 197.
[57] Y. Yamaguchi, Y. Nagasawa, S. Shimomura, K. Tabata, E. Suzuki, Chem Phys Lett 2000, 316, 477.
[58] T. Sahm, A. Gurlo, N. Bârsan, U. Weimar, Sens Actuators B-Chem 2006, 118, 78.
[59] D. S. Vlachos, P. D. Skafidas, J. N. Avaritsiotis, Sens Actuators B-Chem 1995, 25, 491.
[60] J. O. Petunchi, W. K. Hall, J Catal 1983, 80, 403.
[61] L. M. Aparicio, M. A. Ulla, W. S. Millman, J. A. Dumesic, J Catal 1988, 110, 330.
[62] J. R. Huang, G. Y. Li, Z. Y. Huang, X. J. Huang, J. H. Liu, Sens Actuators B-Chem 2006, 114, 1059.
[63] M. J. Fuller, M. E. Warwick, J Catal 1973, 29, 441.
[64] M. Batzill, A. M. Chaka, U. Diebold, Europhys Lett 2004, 65, 61.
[65] F. Parret, P. Menini, A. Martinez, K. Soulantica, A. Maisonnat, B. Chaudret, Sens Actuators B 2006, 118, 276.

Received: 1 January 2011
Revised: 1 September 2011
Accepted: 9 September 2011
Published online on 21 November 2011